Cite this: DOI: 10.1039/c0xx00000x

www.rsc.org/xxxxxx

ARTICLE TYPE

Structural and optical properties of lanthanide oxides grown by atomic layer deposition (*Ln* = Pr, Nd, Sm, Eu, Tb, Dy, Ho, Er, Tm, Yb)

Per-Anders Hansen,*[a] Helmer Fjellvåg,[a] Terje Finstad[b] and Ola Nilsen[a]

Received (in XXX, XXX) Xth XXXXXXXXX 20XX, Accepted Xth XXXXXXXXX 20XX
DOI: 10.1039/b000000x

Ln_2O_3 thin films with optically active f-electrons (*Ln* = Pr, Nd, Sm, Eu, Tb, Dy, Ho, Er, Tm, Yb) have been grown on Si(100) and soda lime glass substrates by atomic layer deposition (ALD) using $Ln(thd)_3$ (Hthd = 2,2,6,6-tetramethyl-3,5-heptanedione) and ozone as precursors. The temperature range for depositions was 200 – 400 °C. Growth rates were measured by spectroscopic ellipsometry and a region with constant growth rate (ALD window) was found for *Ln* = Ho and Tm. All the compounds are grown as amorphous films at low temperatures, whereas crystalline films (cubic C-Ln_2O_3) are obtained above a certain temperature ranging from 300 to 250 °C for Nd_2O_3 to Yb_2O_3, respectively. AFM studies show that the films were smooth (rms < 1 nm) except for depositions at the highest temperatures. Refractive index was measured by spectroscopic ellipsometry and was found to depend on the deposition temperature. Optical absorption measurements show that the absorption from the f-f transitions depends strongly on the crystallinity of the material. The clear correlation between the degree of crystallinity, optical absorptions and refractive index, is discussed.

Introduction

Lanthanide oxides, Ln_2O_3, cover a large range of applications. A partially filled f-shell gives rise to rather unique optical properties. Many phosphors, lasers, LEDs and biological markers are based on these f-f transitions [1, 2]. The oxides have high melting points and are thermodynamically very stable, making them useful as refractory materials and protective coatings [3]. They are furthermore stable in contact with silicon [4], a prerequisite for silicon based technologies. They prevail as various polymorphs, however, the dominating cubic modification frequently enables epitaxial growth, as reported for ALD grown $LaLuO_3$ on GaAs(111) [5] and e-beam evaporated Gd_2O_3 on GaAs(100) [6].

There exist already reviews on ALD growth of lanthanide oxide films [7, 8]. Among the lanthanide oxides and precursors studied in this work, Nd [9] and Er [10] have previously been investigated in the temperature range 200 – 450 °C, Yb [11] at 250 – 400 °C, while for Sm, Eu, Dy, Ho, Tm [8], and Tb [12] only data at 300 °C are available. The use of alternative precursors has been investigated [13-20]. Ternary oxides and nanolaminates containing lanthanides have been deposited both by using the *β*-diketonate chelates $Ln(thd)_3$ (Hthd = 2,2,6,6-tetramethyl-3,5-heptanedione) [9, 12, 21-26] and alternative [27-29] precursors. For the majority of the previous reports, the main focus has been on the electrical properties since ALD lanthanide oxide films are well recognized for their dielectric properties in microelectronics [30, 31]. With respect to optical application of ALD grown lanthanides, $Er(thd)_3$ and $Yb(thd)_3$ have been used to introduce dopants in Y_2O_3 [32-34], and selected lanthanide oxides have been used as optical gain materials in microphotonics [35].

The goal of the present work is twofold; first achieve complete insight into the $Ln(thd)_3$ - ozone precursor system for the entire temperature interval 200 – 400 °C with respect to growth rate and crystallinity; second, to clarify how the deposition temperature affects the optical properties of the grown oxide thin film materials, such as refractive index and optical absorption of f-f transitions.

Experimental

The β-diketonate chelates of the lanthanides, $Ln(thd)_3$, were used as delivered from Strem Chemicals with a purity of > 99.9 %. Ozone was used as the oxygen source. Over the course of this investigation, two different ozone generators were employed. When the generator was changed, several samples were rerun to verify that this did not affect the depositions. One generator, an OT-020 from Ozone Technology, utilized > 99.9 % O_2. The other, a BMT 803N from OSTI inc., used oxygen from an ATF Oxygen Concentrator Module, Sequal Technologies. Nitrogen was used as carrier and purge gas as delivered from a nitrogen generator (Schmidlin UHPN3001 N_2 purifier, > 99.999% N_2 + Ar purity). The films were deposited in an F-120 research-type ALD-reactor (ASM Microchemistry Ltd) in the temperature range 200 – 400 °C. The evaporation temperatures used for the *Ln*-precursors are given in Table 1.

Table 1:
Sublimation temperatures for the $Ln(thd)_3$ precursors.

Ln	Pr	Nd	Sm	Eu	Tb	Dy	Ho	Er	Tm	Yb
T (°C)	155	155	145	145	140	130	130	130	125	122

All depositions consisted of 2000 cycles. Pulse times were kept constant at 1.5 and 4 second respectively for the $Ln(thd)_3$ and O_3 pulse, using purge times of 1.5 s after each precursor pulse. The pulse durations proved to be sufficiently long for proper surface saturation and for purging, in agreement with reports [9-11]. 1.5 x 1.5 cm^2 p-type Si(100) and 2 x 3 cm^2 soda lime glass (SLG) substrates were used. In addition, 0.5 x 4 cm^2 Si(100) strips were placed in the inlet and outlet of the deposition

chamber, some 8 cm apart, to better monitor the gradients of the depositions. The native oxide on the silicon was not removed, but all substrates were cleaned in ethanol and dried using dry pressurized air. All depositions were preceded by an *in-situ* ozone cleaning during 100 cycles of 3 s O_3 pulse and 3 s N_2 purge at the deposition temperature to remove any organic remains.

The phase content and crystallinity was measured with a Siemens D5000 X-ray diffractometer using Cu$K\alpha_1$ radiation as filtered by a Ge(111) monochromator. The film thickness and the refractive index were determined with a J. A. Woollam α-SE spectroscopic ellipsometer, fitting the data to a Cauchy function. Surface morphology R_q was measured with a Park XE70 atomic force microscope (AFM) in tapping mode over a 5x5 μm^2 area. Optical absorption measurements were done on a Shimadzu UV-3600 photospectrometer. SEM analysis was performed on a FEI Nova NanoSEM 650.

Results

During the depositions, it became apparent that the chemistry of the Pr and Tb oxides was different from the other lanthanides at the chosen conditions. While all the other lanthanide oxides appeared as even films with good coverage, the Pr and Tb oxide films showed strong thickness gradients. Pr and Tb were therefore not subjected to a full investigation and are treated separately below. Therefore, in this paper Ln_2O_3 refers to lanthanides with similar chemistries (Ln = Nd, Sm, Ey, Dy, Ho, Er, Tm, Yb). The growth of Yb_2O_3 is presented in more detail as a representative example for the growth of the Ln_2O_3 oxides.

Film growth

Fig. 1 shows the measured growth rates as a function of deposition temperature for the eight studied lanthanide oxides on Si(100) substrates. Comparisons to measurements reported in the literature are included. A well-defined ALD window (temperature independent growth rate) is only noted for the growth of Ho_2O_3 and Tm_2O_3. The growth rates of the other lanthanide oxides increase gradually with temperature.

The growth rate of many lanthanide oxides have been reported for depositions at 300 °C [8, 11] and are mostly in good agreement with our results, see Fig. 2. An exception is the growth rate for the Tb deposition reported in [12] which is much lower than found currently. Unfortunately, few details on the deposition is provided. The surface roughness of the Ln_2O_3 films deposited at 300 °C was determined by AFM. For a fixed number of cycles of 2000, the film thicknesses vary from 100 nm for the light lanthanides to 40 nm for the heavy. Neglecting Pr and Tb, there is an apparent trend where the growth rate and surface roughness decrease for the heavier Ln-elements. The reason for this trend is unknown. The Pr-oxide film was too rough for being investigated well with AFM.

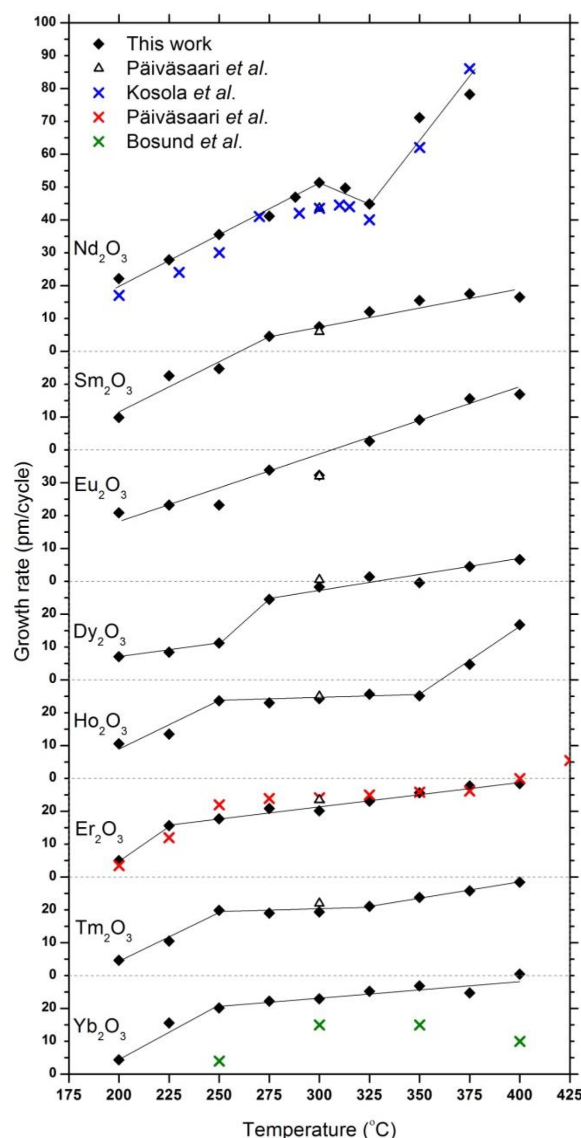

Fig. 1 Growth rates of Ln_2O_3 in comparison to literature data: Ln_2O_3 at 300 °C [8] (open triangles), Nd_2O_3 [9] (blue), Er_2O_3 [10] (red) and Yb_2O_3 [11] (green).

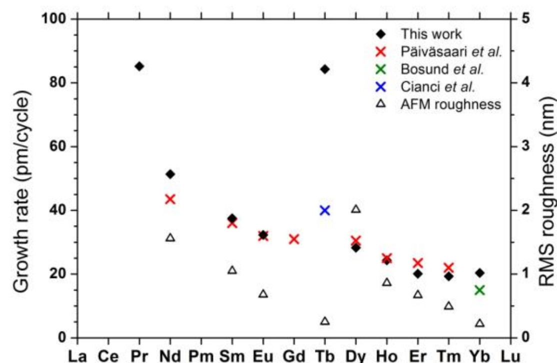

Fig 2 Observed growth rates of lanthanide oxides at 300 °C including values reported by Päiväsaari [8], Bosund [11] and Cianci [12] *et al*. The surface roughness (right axis) of the currently deposited samples as measured by AFM is given by open triangles.

 This journal is © The Royal Society of Chemistry [year]

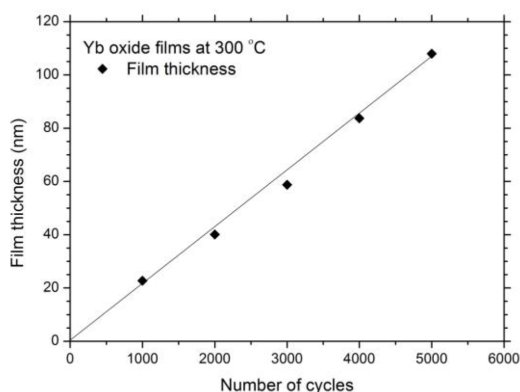

Fig. 3 Yb_2O_3 film thickness for depositions at 300 °C as function of number of deposition cycles.

For Yb_2O_3 grown at 300 °C the film thickness increases linearly between 1000 and 5000 cycles, see Fig. 3. Further, the trend line goes though the origin. The observed linearity suggests that there is no nucleation barrier for growth while the zero offset gives no indication for any nucleation issues at the start of the ALD reaction.

AFM measurements of Yb_2O_3 films show very smooth films with a surface roughness of approximately 0.3 nm for $T \leq 350$ °C. For higher temperatures the roughness steadily increases to 1.4 nm at 400 °C. The film thicknesses of these studied films varied between 30 nm at 225 °C and 60 nm at 400 °C.

Phase content and crystallinity

XRD measurements of all the oxide films deposited at various temperatures are shown in Fig. 6. The data indicates that the lanthanide oxides are amorphous when deposited below a certain temperature, while crystalline films of cubic Ln_2O_3 are obtained above a threshold temperature. This temperature decreases from 300 °C for the early lanthanides to 250 °C for the late lanthanides. Although the diffraction data show signs of oriented growth, there is no strong preference for any particular growth direction. The Bragg reflections match well with those of the cubic Ln_2O_3 structures as reported for Nd and Eu [36], Sm [37], Dy and Ho [38], Er [39] Tm [40] Yb [41], shown as vertical bars in Fig. 6. The reflection marked “Hex.” for Nd_2O_3 match well with the (010) and (-110) reflections of hexagonal Nd_2O_3 [42]. The reflection marked “Mon?” is possibly due to monoclinic Eu_2O_3 [43].

Also Pr and Tb give oxide thin films at 300 °C for the same deposition parameters, however, with inhomogeneous growth. The Pr-oxide samples showed strong thickness gradients throughout the deposition chamber with thicker films towards the gas inlet, while for the Tb-oxides the gradients were moderate. In both cases, variations of the supply of $Pr(thd)_3$ and $Tb(thd)_3$ precursors did not affect the gradients. Neither of the two oxides crystallized in the cubic Ln_2O_3 form, but rather adopted the Ln_6O_{11} [44, 45] and PrO_2 [46] structures as shown in Fig. 4. AFM measurements of Tb-oxide deposited at 300 °C gave a roughness of rms = 0.3 nm, fully in line with the Ln_2O_3 described above. The roughness of the Pr-oxide deposited at the same temperature was, however, impossible to measure by AFM. Fig. 5 shows a FESEM image for such a Pr-oxide surface, containing triangular pyramids of around 50 nm in size. This agrees well with the XRD data in Fig. 4 which show a strong [111] growth preference for the cubic PrO_2 phase.

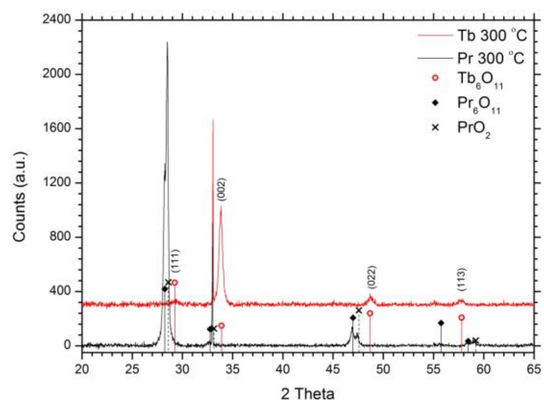

Fig. 4 XRD data for Pr and Tb oxides deposited at 300 °C. The sharp reflection at 2Θ = 33° is from the silicon substrate.

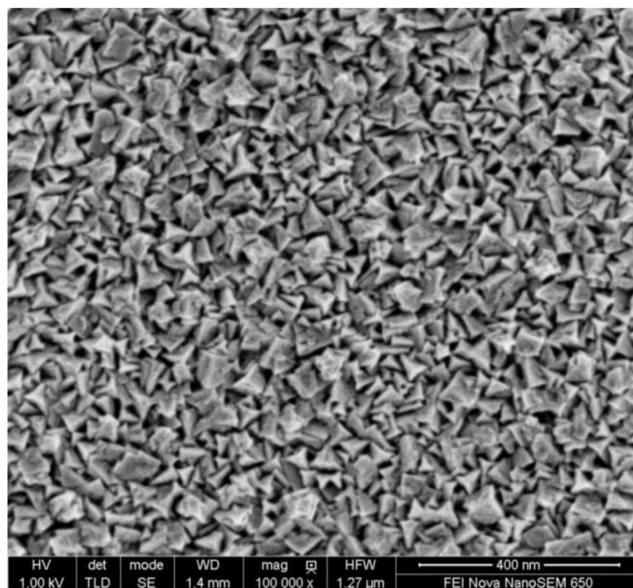

Fig. 5 FESEM picture of a Pr-oxide film deposited at 300 °C.

Cite this: DOI: 10.1039/c0xx00000x

www.rsc.org/xxxxxx

ARTICLE TYPE

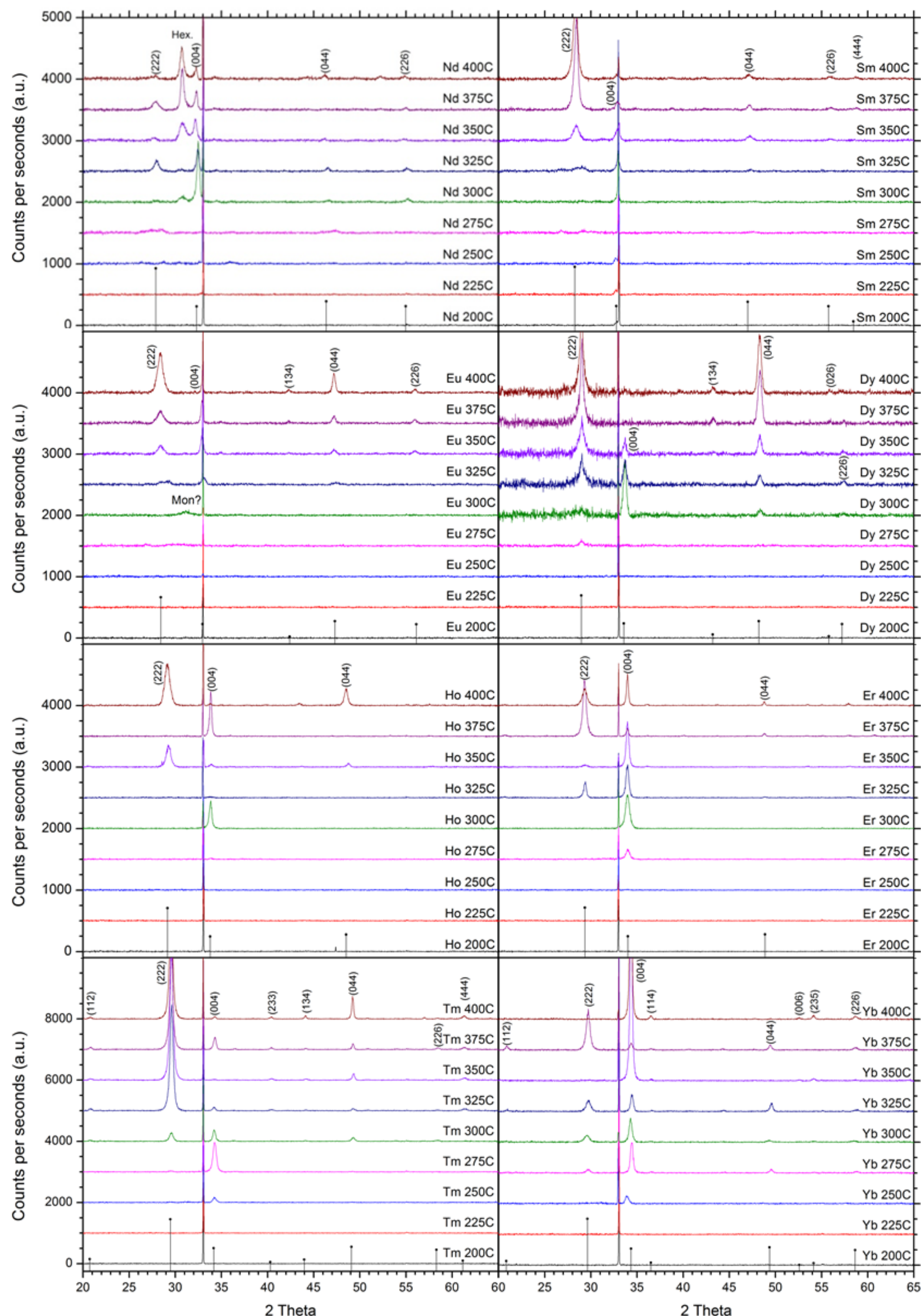

Fig. 6 XRD data for Ln_2O_3 films as function of deposition temperature. The sharp reflection at 2Θ = 33° is from the silicon substrate.

Dynamic Article Links ►

Cite this: DOI: 10.1039/c0xx00000x

www.rsc.org/xxxxxx

ARTICLE TYPE

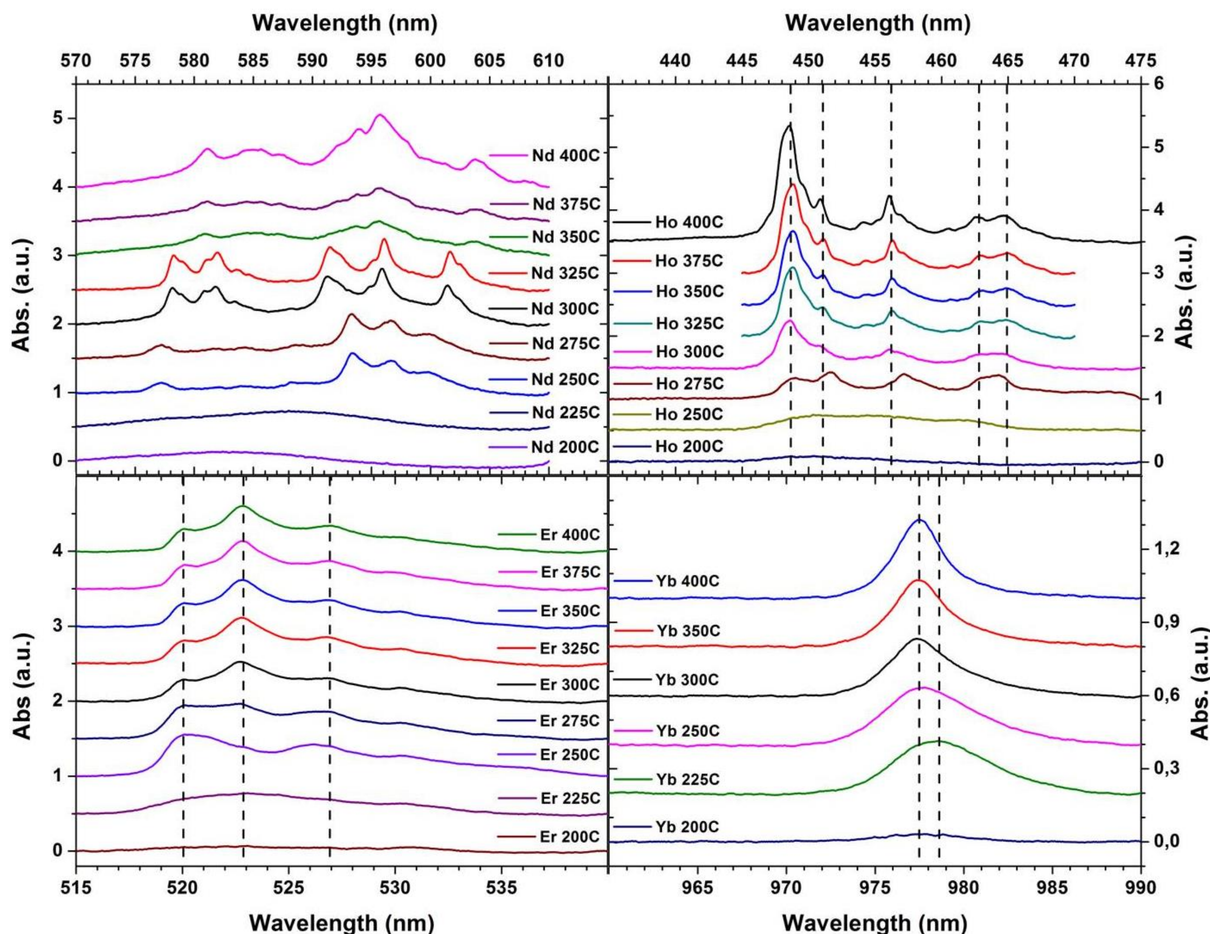

Fig. 7 Optical absorption data for Nd, Ho, Er and Yb oxide films as function of deposition temperatures.

Optical properties

All the currently studied lanthanides have optically active f-f transitions that are generally independent of the host matrix, but can be affected to some degree by the local environments of the cations. Therefore, the optical transmission on glass substrates was measured in order to identify any correlations between deposition temperature and f-f transitions. However, since the absorption from these forbidden transitions is very weak and the films were typically less than 100 nm thick, these transitions were only detectable for the deposited Nd, Ho, Er and Yb oxides, see Fig. 7.

The optical spectra clearly show that the temperature of deposition affects the absorption bands in several ways. For the lowest deposition temperatures, 200-225 °C, the spectra do not exhibit any distinct peaks. For Nd, Ho, Er and Yb, the first clear set of absorption peaks at low temperature changes to a different set at 300, 300, 275 and 250 °C, respectively. This change matches exactly the temperature for onset of growth of crystalline films, see Fig. 6. For the Nd depositions, a third set of peaks appear at 350 °C. This coincides with the appearance of a hexagonal phase in the diffraction pattern for the same deposition temperature.

Fig. 8 shows the refractive index (at 632.8 nm) as function of deposition temperature for the Ln_2O_3-oxides. In parallel with the XRD results, the refractive index exhibits two distinct regions. For deposition temperatures lower than some 275 °C, the refractive index increases with deposition temperature and approach a value of just above 1.9. This plateau value is reached at the same or slightly lower deposition temperatures than the onset of growth of crystalline films.

Cite this: DOI: 10.1039/c0xx00000x

www.rsc.org/xxxxxx

ARTICLE TYPE

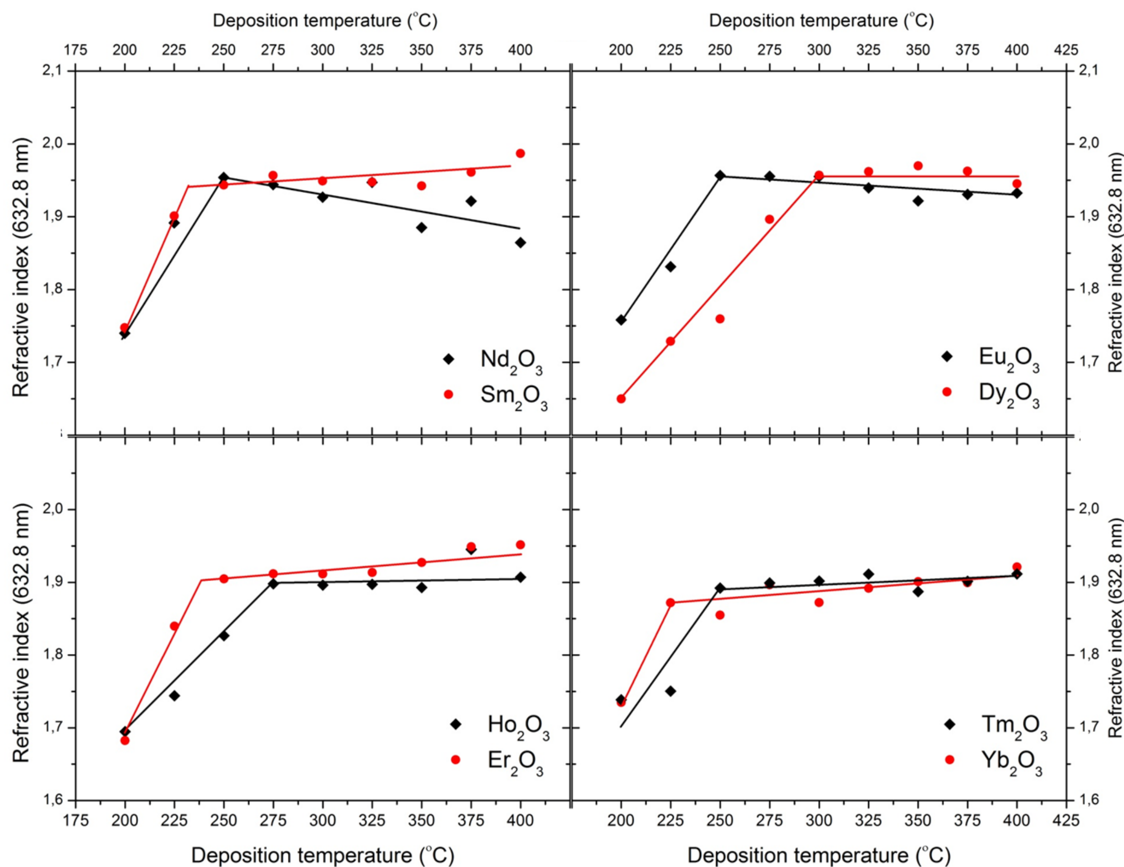

Fig. 8 Refractive index (at 632.6 nm) of Ln_2O_3 oxides as function of deposition temperature.

Discussion

All performed Ln_2O_3 deposition resulted in smooth films, with a growth rate that increases steadily with deposition temperature and is larger for the early lanthanides. Apparently, all these oxide depositions are chemically very similar. A well-defined ALD window is seen only for *Ln* = Ho and Tm. However, a lack of an ALD window does not imply that the deposition is not self-limited. The self-limiting nature was proven by varying the pulsing times as described above.

At low temperatures, all depositions resulted in amorphous films. For deposition temperatures above some 250 and 300 °C crystalline films with the cubic Ln_2O_3 crystal structure are formed, see Fig. 6. This further supports the similarity in chemical behavior of the lanthanide oxides. For *Ln* = Nd a hexagonal phase is obtained in addition to the cubic phase at 350 °C and above. All films are very smooth, even when being crystalline. For Yb_2O_3, the first sign of crystallinity is at 250 °C. These films maintain a surface roughness of approximately 0.3 nm for deposition temperatures up to 350 °C.

Fig. 8 shows that the refractive index increases with increasing deposition temperatures up to some 275 °C, whereafter it stays nearly constant. The transition between these two regimes coincides with the onset temperature for deposition of crystalline films. It is likely that lower surface mobility of the precursor molecules as well for O-atoms bonded to *Ln*-cations, may give rise to amorphous films at low deposition temperature, and that slow diffusion causes a lower material density that furthermore impacts the refractive index. The latter ought to become constant as soon as the films become crystalline.

The deposition of Pr and Tb oxides deviates from the general trends for Ln_2O_3 films. These two elements often adopt mixed Ln^{3+} and Ln^{4+} oxidation states, whereas all other lanthanides prefer the Ln^{3+} state in oxidizing conditions, though with exception of cerium that prefers the Ce^{4+} state. Since ozone is used as the oxygen source, it is likely that Pr and Tb indeed adopts a high oxidation state. This is supported by the XRD results in Fig. 4. The mixed oxidation states makes Pr and Tb (and Ce) oxides catalytically active. It could therefore be possible that ozone oxidizes Tb^{3+} to Tb^{4+} which in turn oxidizes the next pulse of $Tb(thd)_3$, resulting in an enhanced growth rate: The same

could also apply for Pr. This would furthermore explain why such depositions give gradients over the substrates: The surface region closest to the precursor inlet will most probably be more oxidized than the surface near the exhaust vent. There are, however, noticeable differences between the Pr and Tb depositions as the Pr deposition gave highly structured films while the Tb deposition gave very smooth films (like the rest of the lanthanides).

By comparing Fig. 6 and Fig. 7, one observes good correspondence between the changes in positions of the absorption peaks and changes in the crystallinity of the films. This is reasonable since the absorptions originate from forbidden f-f transitions and depend on the local environment around the lanthanide cations. The optical absorption spectra of these films are thus a good probe for the local symmetry around the lanthanide ions. However, the absorptions are weak so high sensitive measurements are required.

Conclusion

Ln_2O_3 films have been deposited in the temperature range 200 – 400 °C. The involved deposition chemistry is very similar and provides very smooth and well controlled films. For low deposition temperatures, the films appear as amorphous while at 250 to 300 °C they adopt a cubic crystalline phase (C-Ln_2O_3). C-Nd_2O_3 occurs as two-phase with a hexagonal polymorph (A-Nd_2O_3) at and above 350 °C. A different behavior was observed for *Ln* = Pr and Tb during depositions with ozone as oxidizer, most probably due to the ability of these lanthanides to form Ln^{3+}/Ln^{4+} mixed phases at these conditions, that resulted in much higher growth rates, less homogeneous films and different crystal structures. Whereas the Tb-films had a very low surface roughness, the Pr-depositions gave highly structured surfaces clearly showing [111] oriented cubic crystallites.

The optical properties of the Ln_2O_3 films can be tuned by selecting the deposition temperature. The refractive index can thereby be tuned from 1.7 to 1.95. The f-electron energy levels depends on the local structure of the lanthanide cations, and hence also on the degree of crystallinity and thereby on the deposition temperature.

This work shows that ALD is most suitable for deposition of the lanthanide oxides; their growth rates are reproducible compared to literature data, the films are smooth and homogeneous, and the optical properties and crystal structure of the films can be tuned by selecting the deposition temperature.

Acknowledgements

We are indebted to the FEI-corporation for acquiring the SEM image. This work was performed within "The Norwegian Research Centre for Solar Cell Technology" project number 193829, a Centre for Environment-friendly Energy Research co-sponsored by the Research Council of Norway and research and industry partners in Norway.

Notes and references

[*] *Email:p.a.hansen@kjemi.uio.no*
[a] *Department of Chemistry, Centre for Materials Science and Nanotechnology, University of Oslo, Sem Sælandsvei 26, 0371 Oslo, Norway*
[b] *Department of Physics, Centre for Materials Science and Nanotechnology, University of Oslo, Sem Sælandsvei 24, 0371 Oslo, Norway*

References

1. J.-C. G. Bünzli, S. Comby, A.-S. Chauvin and C. D. B. Vandevyver, Journal of Rare Earths, 2007, **25**, 257-274.
2. T. Jüstel, H. Nikol and C. Ronda, Angewandte Chemie International Edition, 1998, **37**, 3084-3103.
3. G. Bonnet, M. Lachkar, J. P. Larpin and J. C. Colson, Solid State Ionics, 1994, **72, Part 2**, 344-348.
4. K. J. H. a. D. G. Schlom, Journal of Materials Research, 1996, **11**, 2757-2776.
5. Y. Liu, M. Xu, J. Heo, P. D. Ye and R. G. Gordon, Applied Physics Letters, 2010, **97**, 162910-162910-162913.
6. M. Hong, J. Kwo, A. R. Kortan, J. P. Mannaerts and A. M. Sergent, Science, 1999, **283**, 1897-1900.
7. A. C. Jones, H. C. Aspinall, P. R. Chalker, R. J. Potter, K. Kukli, A. Rahtu, M. Ritala and M. Leskelä, Materials Science and Engineering B, 2005, **118**, 97-104.
8. J. Päiväsaari, M. Putkonen and L. Niinistö, Thin Solid Films, 2005, **472**, 275-281.
9. A. Kosola, J. Päiväsaari, M. Putkonen and L. Niinistö, Thin Solid Films, 2005, **479**, 152-159.
10. J. Päiväsaari, M. Putkonen, T. Sajavaara and L. Niinistö, Journal of Alloys and Compounds, 2004, **374**, 124-128.
11. M. Bosund, K. Mizohata, T. Hakkarainen, M. Putkonen, M. Söderlund, S. Honkanen and H. Lipsanen, Applied Surface Science, 2009, **256**, 847-851.
12. E. Cianci, A. Lamperti, G. Congedo and S. Spiga, ECS Journal of Solid State Science and Technology, 2012, **1**, P5-P10.
13. K. Kukli, M. Ritala, T. Pilvi, T. Sajavaara, M. Leskela, A. C. Jones, H. C. Aspinall, D. C. Gilmer and P. J. Tobin, Chemistry of Materials, 2004, **16**, 5162-5168.
14. H. Kondo, M. Sakashita and S. Zaima, Journal of the Vacuum Society of Japan, 2011, **54**, 110-113.
15. R. J. Potter, P. R. Chalker, T. D. Manning, H. C. Aspinall, Y. F. Loo, A. C. Jones, L. M. Smith, G. W. Critchlow and M. Schumacher, Chemical Vapor Deposition, 2005, **11**, 159-169.
16. J. Päiväsaari, J. Niinistö, K. Arstila, K. Kukli, M. Putkonen and L. Niinistö, Chemical Vapor Deposition, 2005, **11**, 415-419.
17. R. Xu, Q. Tao, Y. Yang and C. G. Takoudis, Applied Surface Science, 2012, **258**, 8514-8520.
18. K. Xu, R. Ranjith, A. Laha, H. Parala, A. P. Milanov, R. A. Fischer, E. Bugiel, J. Feydt, S. Irsen, T. Toader, C. Bock, D. Rogalla, H.-J. Osten, U. Kunze and A. Devi, Chemistry of Materials, 2012, **24**, 651-658.
19. M. Malvestuto, G. Scarel, C. Wiemer, M. Fanciulli, F. D'Acapito and F. Boscherini, Nuclear Instruments and Methods in Physics Research Section B: Beam Interactions with Materials and Atoms, 2006, **246**, 90-95.
20. J. Paivasaari, I. V. C. L. Dezelah, D. Back, H. M. El-Kaderi, M. J. Heeg, M. Putkonen, L. Niinisto and C. H. Winter, Journal of Materials Chemistry, 2005, **15**, 4224-4233.
21. A. Tamm, M. Heikkilä, M. Kemell, J. Kozlova, K. Kukli, V. Sammelselg, M. Ritala and M. Leskelä, Thin Solid Films, 2010, **519**, 666-673.

22. J. J. Montiel i Ponsoda, L. Norin, C. Ye, M. Bosund, M. J. Söderlund, A. Tervonen and S. Honkanen, Opt. Express, 2012, **20**, 25085-25095.
23. B. Toomey, K. Cherkaoui, S. Monaghan, V. Djara, É. O'Connor, D. O'Connell, L. Oberbeck, E. Tois, T. Blomberg, S. B. Newcomb and P. K. Hurley, Microelectronic Engineering, 2012, **94**, 7-10.
24. P. Myllymaki, M. Roeckerath, J. M. Lopes, J. Schubert, K. Mizohata, M. Putkonen and L. Niinisto, Journal of Materials Chemistry, 2010, **20**, 4207-4212.
25. C. Adelmann, J. Swerts, O. Richard, T. Conard, M. Popovici, J. Meersschaut, V. V. Afanas'ev, L. Breuil, A. Cacciato, K. Opsomer, B. Brijs, H. Tielens, G. Pourtois, H. Bender, M. Jurczak, J. V. Houdt, S. V. Elshocht and J. A. Kittl, Journal of The Electrochemical Society, 2011, **158**, H778-H784.
26. K. Uusi-Esko and M. Karppinen, Chemistry of Materials, 2011, **23**, 1835-1840.
27. R. Xu, ECS journal of solid state science and technology, 2012, **1**, N107.
28. J. M. Gaskell, S. Przybylak, A. C. Jones, H. C. Aspinall, P. R. Chalker, K. Black, R. J. Potter, P. Taechakumput and S. Taylor, Chemistry of Materials, 2007, **19**, 4796-4803.
29. P. de Rouffignac and R. G. Gordon, Chemical Vapor Deposition, 2006, **12**, 152-157.
30. N. A. Stafford, R. Katamreddy, L. Guerin, B. Feist, C. Dussarrat, V. Pallem, C. Weiland and R. Opila, ECS Transactions, 2009, **19**, 525-536.
31. C. Wiemer, L. Lamagna and M. Fanciulli, Semiconductor Science and Technology, 2012, **27**, 074013.
32. J. Hoang, R. N. Schwartz, K. L. Wang and J. P. Chang, Journal of Applied Physics, 2012, **112**, 063117-063111.
33. J. Hoang, R. N. Schwartz, K. L. Wang and J. P. Chang, Journal of Applied Physics, 2012, **112**, 023116-023116.
34. J. Hoang, T. T. Van, M. Sawkar-Mathur, B. Hoex, M. C. M. V. d. Sanden, W. M. M. Kessels, R. Ostroumov, K. L. Wang, J. R. Bargar and J. P. Chang, Journal of Applied Physics, 2007, **101**, 123116.
35. C. P. Michael, H. B. Yuen, V. A. Sabnis, T. J. Johnson, R. Sewell, R. Smith, A. Jamora, A. Clark, S. Semans, P. B. Atanackovic and O. Painter, Opt. Express, 2008, **16**, 19649-19666.
36. H. Bommer, Z Anorg Allg Chem, 1939, **241**, 273-280.
37. A. Bartos, K. P. Lieb, M. Uhrmacher and D. Wiarda, Acta Crystallogr B, 1993, **49**, 783-783.
38. E. N. Maslen, V. A. Streltsov and N. Ishizawa, Acta Crystallogr B, 1996, **52**, 414-422.
39. Y. A. Malinowskii and O. S. Bondareva, Kristallografiya+, 1991, **36**, 1558-1560.
40. J. Blanusa, M. Mitric, D. Rodic, A. Szytula and M. Slaski, J Magn Magn Mater, 2000, **213**, 75-81.
41. G. Will, N. Masciocchi, M. Hart and W. Parrish, Acta Crystallogr A, 1987, **43**, 677-683.
42. P. Aldebert and J. P. Traverse, Materials Research Bulletin, 1979, **14**, 303-323.
43. G. Chen, J. R. Peterson and K. E. Brister, Journal of Solid State Chemistry, 1994, **113**, 451-451.
44. E. D. Guth and L. Eyring, Journal of the American Chemical Society, 1954, **76**, 5242-5244.
45. J. Zhang, R. B. VonDreele and L. Eyring, Journal of Solid State Chemistry, 1996, **122**, 53-58.
46. A. F. Andreeva, I. Y. Gilman, M. Y. Gamarnik and V. I. Dekhtyaruk, Inorg Mater+, 1986, **22**, 1155-1160.

This journal is © The Royal Society of Chemistry [year]